A Theoretical Study on the Electronic and Vibrational Structure of the Phenoxyl Radical

Junko TAKAHASHI,* Takamasa MOMOSE, and Tadamasa SHIDA
Department of Chemistry, Faculty of Science, Kyoto University, Kyoto 606-01
(Received October 25, 1993)

The electronic structures of the phenoxyl radical in the electronic ground and excited states are studied by ab initio MO calculations. The geometries are optimized by the CAS-MCSCF procedure with the Huzinaga–Dunning DZV basis set. The electronic excitation energies and transition dipole moments are calculated by the CI procedure. According to the result of the calculation the observed absorption bands at about 600, 400, and 300 nm are assigned as $\tilde{X}^2B_1 \rightarrow \tilde{1}^2B_2$ ($n \rightarrow \pi$), $\tilde{X}^2B_1 \rightarrow \tilde{1}^2A_2$ and $\tilde{2}^2B_1$ ($\pi \rightarrow \pi^*$), and $\tilde{X}^2B_1 \rightarrow \tilde{2}^2A_2$, respectively. In order to analyze the vibrational character of the absorption band at about 400 nm the force constants, the potential energy distributions, the normal modes, and the Franck–Condon integrals are calculated for the three states, $\tilde{X}^2B_1$, $\tilde{1}^2A_2$, $\tilde{2}^2B_1$. The force constants are scaled by referring to the experimental resonance Raman, Trapped Ion Photodissociation (TIP), and the matrix-isolated electronic absorption spectra. The strongest vibrational band of the TIP and the absorption spectra is assigned to the 0–0 band of the $\tilde{X} \rightarrow \tilde{1}^2A_2$ transition and the second strongest, at a higher energy of 1110 cm^{-1}, to the 0–0 band of the $\tilde{X} \rightarrow \tilde{2}^2B_1$ transition. The theoretical vibronic absorption and Raman spectra are reproduced and compared favorably with the experimental spectra.

As reviewed recently[1] the benzyl radical has been studied by a number of authors.[2—26] The radical exhibits a weak absorption band at ca. 450 nm which is regarded as due to the two transitions $\tilde{X} \rightarrow \tilde{1}^2A_2$ and $\tilde{X} \rightarrow \tilde{2}^2B_1$ strongly coupled by the vibronic interaction. There are two more π–π^* transitions in the UV region, one at ca. 320 nm with a medium intensity and the other at ca. 270 nm with a strong intensity.[27—30]

The phenoxyl radical has also been the subject of several studies because it is a seven π electron system similar to the benzyl radical.[31—43] Experimentally, it is reported that the phenoxyl radical exhibits a weak and a strong absorption band at about 400 and 300 nm.[31—33,35] Therefore, it is reasonable to expect that the bands correspond to the ca. 450 nm and the ca. 320 nm bands of the benzyl radical. A difference between the two radicals is that in the phenoxyl radical an additional transition of $n \rightarrow \pi^*$ character involving the in-plane non-bonding electrons on the oxygen atom is possible, which is claimed to be seen very faintly at about 600 nm by Ward[34] and Pullin and Andrews.[35]

In the present work the electronic structure of the phenoxyl radical is studied by ab initio MO calculations. The vibronic structure of the ca. 400 nm band is analyzed by calculating the force constants and the Franck–Condon integrals for the three states $\tilde{X}$, $\tilde{1}^2A_2$, and $\tilde{2}^2B_1$. As a result, it is concluded that the band at ca. 400 nm is to be regarded as an overlap of the transitions of $\tilde{X} \rightarrow \tilde{1}^2A_2$ and $\tilde{X} \rightarrow \tilde{2}^2B_1$ without any significant vibronic coupling contrary to the case of the ca. 450 nm band of the benzyl radical.

The band at ca. 400 nm of the phenoxyl radical is also studied in the gas phase by Trapped Ion Photodissociation (TIP) spectroscopy by Mikami et al.[40] The resonance Raman spectrum induced by the excitation with photons of 399 nm is investigated in detail by Tripathi and Schuler.[38] These spectra are utilized for the scaling of the ab initio force constants to reproduce the vibronic feature and the Raman spectrum.

The mode mixing effect between the ground state and the excited state, namely the Duschinsky effect, must be taken into account when the Franck–Condon integrals are calculated to compare the available experimental spectra. In the present work we use the recurrence formulae derived by Momose and Shida[48,49] for the calculation of the multidimensional Franck–Condon integrals.

In the following section the geometry optimization and the calculation of electronic transition energy and transition dipole moment are performed first. Then, the vibronic structure of the band at about 400 nm is analyzed by performing the calculation of the ab initio force constants and Franck–Condon integrals and by comparing with the experimental TIP and resonance Raman spectra. In the final section the conclusions of the present work are summarized.

Electronic Analysis

Geometry Optimization. The numbering of atom and the geometrical parameters are shown in Fig. 1.

The geometry optimization for the electronic ground and the first two $\pi \rightarrow \pi^*$ excited states are carried out by the CAS-MCSCF method with the basis set of Huzinaga–Dunning DZV; (9s5p/4s)/[3s2p/2s], employing the HONDO7 program.[44] Seven π and π^* and one n orbitals shown in Fig. 2 are chosen as the active space where n stands for the in-plane non-bonding orbital of the oxygen atom perpendicular to the C–O bond.

The configurations for the MCSCF wave function are generated by distributing nine electrons in these eight orbitals. The total number of configuration state functions is 1274 in the C_s symmetry (planar structure). The optimized geometries are listed in Table 1. All the

Table 1. Optimized Geometries of the Phenoxyl Radical

Electronic state	$\tilde{X}^2B_1$	$\tilde{1}^2A_2$	$\tilde{2}^2B_1$
Total energy/hartree	−304.9628358	−304.8706713	−304.8560822
Bond length/Å			
C_1–O	1.2953	1.2510	1.3624
C_1–C_2	1.4413	1.4681	1.4537
C_2–C_3	1.3925	1.4511	1.3772
C_3–C_4	1.4181	1.4097	1.4640
C_2–H	1.0709	1.0707	1.0710
C_3–H	1.0713	1.0710	1.0711
C_4–H	1.0710	1.0695	1.0696
Bond angle/degree			
$C_6C_1C_2$	118.89	115.19	120.20
$C_1C_2C_3$	120.07	121.44	119.91
$C_2C_3C_4$	120.38	121.42	120.56
$C_3C_4C_5$	120.21	119.09	118.86

The geometry optimization is performed by the CAS-MCSCF method with the Huzinaga–Dunning DZV basis set. The active orbitals are seven π orbitals and one in-plane lone pair orbital on the oxygen atom. The total number of configurations is 1274 in the C_s symmetry.

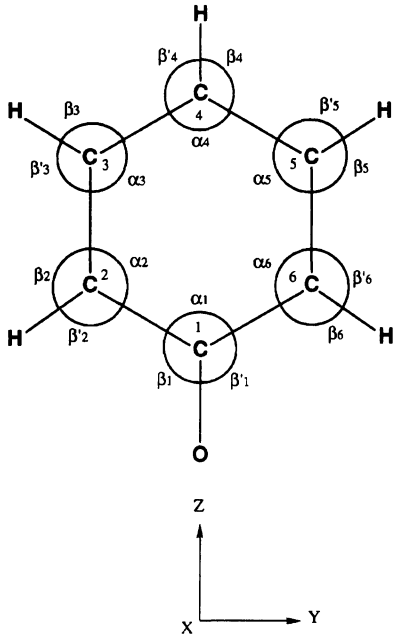

Fig. 1. Coordinate system of the phenoxyl radical.

three states converged are of the C_{2v} symmetry. r(C–O) of 1.2510 Å for $\tilde{1}^2A_2$ and of 1.3624 Å for $\tilde{2}^2B_1$ are very close to the standard length of the C–O double and single bonds, respectively, while r(C–O) of 1.2953 Å for the ground state is just about in-between. In the ground state $r(C_1–C_2)$ and $r(C_3–C_4)$ are longer than $r(C_2–C_3)$. The same holds for $\tilde{2}^2B_1$ with even larger differences between the two groups of the bond lengths. In contrast, $r(C_2–C_3)$ in $\tilde{1}$ becomes markedly longer than the other two states. With these bond lengths the character of $\tilde{1}$ may be regarded as a relatively weak composite of the conjugative units of $C_2C_1(O)C_6$ and $C_3C_4C_5$ while that of $\tilde{2}$ as a composite of six carbon π electrons and one relatively isolated oxygen π electron.

Recently, Liu and Zhou calculated the geometry of the phenoxyl radical in the ground state by the UNO-CAS procedure with the 6-31G* basis set and obtained 1.239, 1.452, 1.378, and 1.413 Å for r(C–O), $r(C_1–C_2)$, $r(C_2–C_3)$, and $r(C_3–C_4)$, respectively.[43] The main difference between their result and the present result is that the value of r(C–O) is shorter by about 0.056 Å in the former. It reflects the general trend that the inclusion of polarization functions shortens the bond length of the carbonyl group.

Electronic Transition Energies and Transition Dipole Moments. The transition energies are calculated for the optimized ground state geometry by the following three methods; 1) MR-SD-CI calculation with the DZV basis set, 2) CAS-CI calculation using the natural orbitals of the CAS-MCSCF wave function with the DZV basis set, 3) CAS-CI calculation in a similar manner as 2) with the basis set of DZV plus a polarization function on the oxygen atom. In the MR-SD-CI calculation the reference configurations are selected by the criterion that the CI coefficients exceed 0.1. They include $[---(1b_1)^2(2b_1)^2\ (8b_2)^2\ (3b_1)^1\ (1a_2)^2]$, $[---(1b_1)^2\ (2b_1)^1\ (8b_2)^2\ (3b_1)^2\ (1a_2)^2]$, $[---\ (1b_1)^2\ (2b_1)^1\ (8b_2)^2\ (3b_1)^1\ (1a_2)^2\ (4b_1)^1]$, $[---(1b_1)^2\ (2b_1)^2\ (8b_2)^2\ (3b_1)^0\ (1a_2)^2\ (4b_1)^1]$, $[---(1b_1)^2\ (2b_1)^2\ (8b_2)^2\ (3b_1)^1\ (1a_2)^1\ (2a_2)^1]$, and $[---\ (1b_1)^2\ (2b_1)^1\ (8b_2)^2\ (3b_1)^1\ (1a_2)^1\ (2a_2)^1\ (4b_1)^1]$ for the $^2B_1$ states, and $[---(1b_1)^2\ (2b_1)^2\ (8b_2)^2\ (3b_1)^2\ (1a_2)^1]$, $[---\ (1b_1)^2\ (2b_1)^2\ (8b_2)^2\ (3b_1)^0\ (1a_2)^2\ (2a_2)^1]$, $[---(1b_1)^2\ (2b_1)^1\ (8b_2)^2\ (3b_1)^1\ (1a_2)^2\ (2a_2)^1]$, $[,---\ (1b_1)^1\ (2b_1)^2\ (8b_2)^2\ (3b_1)^1\ (1a_2)^2\ (2a_2)^1]$, $[---\ (1b_1)^2\ (2b_1)^2\ (8b_2)^2\ (3b_1)^1\ (1a_2)^1\ (4b_1)^1]$, and $[---\ (1b_1)^2\ (2b_1)^2\ (8b_2)^2\ (3b_1)^1\ (1a_2)^1\ (5b_1)^1]$ for the $^2A_2$ states, and $[---\ (7b_2)^2\ (1b_1)^2\ (2b_1)^2\ (8b_2)^1\ (3b_1)^2(1a_2)^2]$ and $[---(7b_2)^1\ (1b_1)^2\ (2b_1)^2\ (8b_2)^2\ (3b_1)^2\ (1a_2)^2]$ for the $^2B_2$ state. All the single and the double excitations from the reference configurations are included. As a result of the

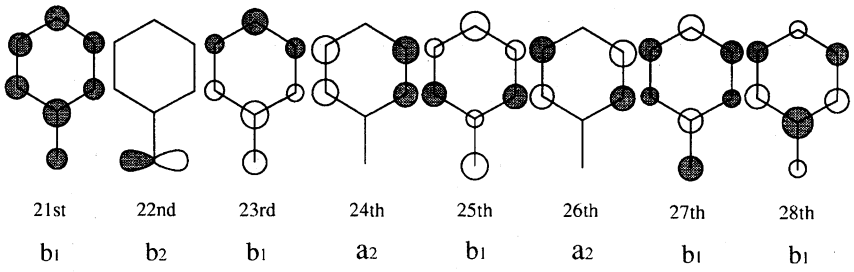

Fig. 2. Active MO's in the CAS-MCSCF calculation.

Table 2. Electronic Transition Energies, Transition Moments, Oscillator Strengths, and the Assignment of the Electronic Absorption Bands of the Phenoxyl Radical

Electronic state	Transition	Transition energy/eV			Transition moment/a.u.	Oscillator strength	Wavelength /nm	Experimental /nm
		Method(1)[a]	Method(2)[b]	Method(3)[c]	method(1)	method(1)	method(1)	
$\tilde{X}^2B_1$	—	—	—	—		—	—	
$\tilde{1}^2B_2$	1st n–π	1.573	—	—		0	788.2	ca. 600
$\tilde{1}^2A_2$	1st π–π^*	2.948	2.979	3.095	0.37950	1.560×10^{-2}	420.5	ca. 400
$\tilde{2}^2B_1$	2nd π–π^*	3.265	3.260	3.248	0.26480	0.841×10^{-2}	379.7	ca. 400
$\tilde{1}^4B_1$	3rd π–π^*	4.083	4.432	4.407	0	0	303.7	
$\tilde{3}^2B_1$	4th π–π^*	5.158	5.135	5.164	0.04093	0.032×10^{-2}	240.4	
$\tilde{2}^2A_2$	5th π–π^*	5.758	5.921	5.722	0.25564	5.409×10^{-2}	215.3	ca. 300

a) MR-SD-CI calculation with the DZV basis set. b) CAS-CI calculation using the natural orbitals of the CAS-MCSCF wave function with the DZV basis set. c) CAS-CI calculation in a similar manner as method (2) with the basis set of DZV plus a polarization function on the oxygen atom.

perturbation selection, the number of the configurations in the CI wave function is reduced to 30000—50000. In the CAS-CI calculation the active space is the same as in the MCSCF calculation described in the preceding subsection and the full-CI calculation within the active space is carried out, where the natural orbitals of the MCSCF wave function for the ground state are used as the one particle bases functions.

The transition dipole moments are also calculated using the CI wave function obtained by method(1), and the oscillator strengths for the excitations are calculated. The program MELDF[45] is used for the CI calculations. The results of the calculation of the electronic transition energies and the oscillator strengths are shown in Table 2.

The accuracy of the calculated transition energies should increase in the order of method(1) < method(2) < method(3). However, the result in Table 2 indicates that the difference among the three is relatively small. The lowest excitation is calculated to be the $\tilde{X}^2B_1 \rightarrow \tilde{1}^2B_2(n\rightarrow\pi)$ transition which involves the in-plane non-bonding orbital on the oxygen atom. The very weak band at about 600 nm in the experimental absorption spectrum[34,35] is assigned to this transition which is forbidden but is observed through the vibronic coupling. The 1st and the 2nd $\pi\rightarrow\pi^*$ transition are $\tilde{X}^2B_1 \rightarrow \tilde{1}^2A_2$ and $\tilde{X}^2B_1 \rightarrow \tilde{2}^2B_1$, respectively. The difference of the energy between the two transitions is only 1234 cm^{-1} (=3.248—3.095 eV) by the best method of (3), which is small enough for the two bands to be regarded as if they constituted a single vibronic band. The 3rd $\pi\rightarrow\pi^*$ excited state is found to be the 1st quartet B_1 state. The 4th and 5th $\pi\rightarrow\pi^*$ excited states are the 3rd $^2B_1$ state and the 2nd $^2A_2$ state, respectively.

As is described above the energy difference between the two transitions $\tilde{X}\rightarrow\tilde{1}^2A_2$ and $\tilde{2}^2B_1$ is relatively small amounting to only 1234 cm^{-1}. This situation is similar to the benzyl radical where the energy difference is even smaller, say, about 450 cm^{-1}.[8] Therefore, one might consider that an extensive vibronic coupling might prevail in the phenoxyl radical also. However, as will be discussed in the following section, the vibronic bands of the two transitions of the phenoxyl radical can be reproduced fairly well simply by the superposition of the vibronic bands belonging to the two transitions $\tilde{X}\rightarrow\tilde{1}^2A_2$ and $\tilde{2}^2B_1$, which implies little vibronic coupling in the phenoxyl radical. The reason for this discrepancy between the two radicals will be discussed later.

Vibrational Analysis

Recapitulation of Calculational Methods. Out of the total 30 vibrational modes the totally symmetric 21 modes will be treated under the assumption that the vibrational feature in both TIP and resonance Raman spectra is mainly determined by these modes.

The Cartesian force constant matrix elements H_{ij} are calculated by differentiation of the energy gradient with the Cartesian displacement chosen as 0.01 bohr. The energy gradients are calculated by the CAS-MCSCF method with the same basis set and the active

Table 3. Symmetrized Internal Coordinates of the Phenoxyl Radical

Stretching coordinates			Skeletal bending coordinates		
1:	C_1–O	(R_1)	13:	$2\alpha_1-\alpha_2-\alpha_3+2\alpha_4-\alpha_5-\alpha_6$	(α_1)
2:	C_2–H	(R_2)	14:	$\alpha_1-\alpha_2+\alpha_3-\alpha_4+\alpha_5-\alpha_6$	(α_2)
3:	C_3–H	(R_3)	15:	$\alpha_2-\alpha_3+\alpha_5-\alpha_6$	(α_3)
4:	C_4–H	(R_4)			
5:	C_5–H	(R_3)	C–H bending coordinates		
6:	C_6–H	(R_2)	16:	$\beta_1-\beta'_1$	(β_1)
7:	C_1–C_2	(R_5)	17:	$\beta_2-\beta'_2$	(β_2)
8:	C_2–C_3	(R_6)	18:	$\beta_3-\beta'_3$	(β_3)
9:	C_3–C_4	(R_7)	19:	$\beta_4-\beta'_4$	(β_4)
10:	C_4–C_5	(R_7)	20:	$\beta_5-\beta'_5$	(β_3)
11:	C_5–C_6	(R_6)	21:	$\beta_6-\beta'_6$	(β_2)
12:	C_6–C_1	(R_5)			

The stretching coordinates and the C–H bending coordinates are classified into seven and four groups on account of the C_{2v} symmetry. The symbols in parentheses are the indices for the classification.

orbitals as in the geometry optimization. Diagonalizing the mass-weighted Cartesian force constant matrix yields 21 eigenvalues for the in-plane normal modes, 9 for the out-of-plane modes, and 6 zero eigenvalues for the translational and rotational degrees of freedom. Since the Cartesian force constants calculated above include those for the translational and rotational motions, they are eliminated by using Williams' projection operator $\boldsymbol{P}$ in Eq. 1.[46]

$$\boldsymbol{P} = \tilde{\boldsymbol{B}}(\boldsymbol{B}\tilde{\boldsymbol{B}})^{-1}\boldsymbol{B}, \tag{1}$$

where $\boldsymbol{B}$ is the matrix that transforms the Cartesian into the internal coordinate system. The Cartesian force constant matrix from which the superfluous contributions are projected out is derived from the original force constant matrix $\boldsymbol{H}$ by Eq. 2

$$\boldsymbol{K} = \boldsymbol{PHP}. \tag{2}$$

Then, the eigenvectors and eigenvalues for the normal modes are calculated by diagonalization of the mass-weighted, projected out Cartesian force constant matrix. The internal force constant matrix $\boldsymbol{F}$ is related with $\boldsymbol{K}$ by the following equation.

$$\boldsymbol{K} = \tilde{\boldsymbol{B}}\boldsymbol{F}\boldsymbol{B}. \tag{3}$$

The internal coordinates used for the calculation of the in-plane normal modes are listed in Table 3. These are selected by the condition of eliminating the redundancy according to Pulay et al.[47]

To obtain better compromised force fields the ab initio internal force constants F_{ij} is scaled as usual by Eq. 4;

$$\mathscr{F}_{ij} = (C_iC_j)^{1/2}F_{ij} \tag{4}$$

where C_i and C_j are the scaling factors for the internal coordinates i and j, respectively. The scaled Cartesian force constant matrix is calculated as

$$\mathscr{K} = \tilde{\boldsymbol{B}}\mathscr{F}\boldsymbol{B} \tag{5}$$

Diagonalization of $\mathscr{K}$ gives the scaled frequencies for the normal modes.

For the characterization of the normal modes it is useful to calculate the potential energy distribution (PED) which is a measure of the distribution of the potential energy of the normal vibration onto the internal coordinates. PED is defined by Eq. 6

$$(\mathrm{PED})_{ia} = \mathscr{F}_{ii}l_{ia}^2/\lambda_a \tag{6}$$

where l and λ are the eigenvectors and eigenvalues of $\mathscr{F}$.

The multidimensional Franck–Condon integrals within the harmonic approximation and with the Duschinsky effect being taken into account are calculated as follows:[48,49] The normal mode of the ground state ($\boldsymbol{Q}^{\mathrm{G}}$) and that of the excited state ($\boldsymbol{Q}^{\mathrm{E}}$) are related as

$$\boldsymbol{Q}^{\mathrm{E}} = \boldsymbol{W}\boldsymbol{Q}^{\mathrm{G}} + \boldsymbol{k}^{\mathrm{E}} \tag{7}$$

where $\boldsymbol{W}$ is the Duschinsky rotation matrix and $\boldsymbol{k}^{\mathrm{E}}$ is the displacement vector of the potential minima of the ground state projected on the normal coordinates for the excited state. The matrix $\boldsymbol{W}$ and the vector $\boldsymbol{k}^{\mathrm{E}}$ are given as

$$\boldsymbol{W} = \tilde{\boldsymbol{L}}^{\mathrm{E}}\boldsymbol{L}^{\mathrm{G}} \tag{8}$$

$$\boldsymbol{k}^{\mathrm{E}} = \tilde{\boldsymbol{L}}^{\mathrm{E}}M^{\frac{1}{2}}(\boldsymbol{X}^{\mathrm{G}}_{\mathrm{eq}} - \boldsymbol{X}^{\mathrm{E}}_{\mathrm{eq}}) \tag{9}$$

where $\boldsymbol{L}^{\mathrm{G}}$ and $\tilde{\boldsymbol{L}}^{\mathrm{E}}$ are the eigenvector of the mass-weighted, projected out Cartesian force constant matrix for the ground state and its transposition for the excited state, respectively. $\boldsymbol{X}^{\mathrm{G}}_{\mathrm{eq}}$ and $\boldsymbol{X}^{\mathrm{E}}_{\mathrm{eq}}$ are the equilibrium geometries in the Cartesian coordinate for the ground state and the excited state, respectively.

The multidimensional Franck–Condon integrals are calculated by the following recurrence formula,[48,49]

$$(m_\mu+1)\boldsymbol{J}\binom{m_\mu+1}{n_\mu} = d_\mu\left(\frac{m_\mu+1}{2}\right)\boldsymbol{J}\binom{m_\mu}{n_\mu} + \sum_{i=l}^{N} a_{\mu i}[m_i(m_\mu+1)]^{\frac{1}{2}}\boldsymbol{J}\binom{m_i-1}{n_i}$$

$$+\frac{1}{2}\sum_{i=1}^{N} c_{\mu i}[n_i(m_\mu+1)]^{\frac{1}{2}} \boldsymbol{J}\binom{m_i}{n_i-1} \quad (10)$$

where $\boldsymbol{J}\binom{m_\mu+1}{n_\mu}$ is the multidimensional Franck–Condon integral for the case where the occupation number for mode μ in the excited state is increased by one and the occupation numbers for the other modes in the excited state as well as all modes in the ground state remain unchanged. The coefficients in Eq. 9 are given as

$$a_{ij} = (2\beta\alpha\tilde{\beta} - 1)_{ij} \quad (11a)$$

$$c_{ij} = (4\beta\alpha)_{ij} \quad (11b)$$

$$d_i = [2\tilde{\kappa}(1 - \beta\alpha\tilde{\beta})]_i \quad (11c)$$

$$\beta = \gamma_{\mathrm{E}}^{\frac{1}{2}} \boldsymbol{W} \gamma_{\mathrm{G}}^{-\frac{1}{2}} \quad (11d)$$

$$\kappa = \gamma_{\mathrm{E}}^{\frac{1}{2}} \boldsymbol{k}^{\mathrm{E}} \quad (11e)$$

$$\alpha = (1 + \tilde{\beta}\beta)^{-1} \quad (11f)$$

where γ_{G} and γ_{E} are the frequency matrix for the normal modes in the ground state and excited state, respectively.[48,49]

Normal Modes of the Ground State. The transient Raman spectra resonant to the 400 nm band of the phenoxyl radical, its isotopomeric radicals, and the para-substituted phenoxyl radicals are reported by Tripathi and Schuler.[38,39] The observed frequencies are used for the scaling of the internal force constants calculated for the ground electronic state. The result of the calculation for the normal modes of the phenoxyl and its isotopomeric radicals in the ground state are shown in Table 4. Figure 3 shows eight relevant normal vibrations.

As shown in Table 4 there are three totally symmetric (a_1) and two non-totally symmetric (b_2) C–H stretching modes in the region above 2000 cm^{-1} which are not observed in the resonance Raman spectrum for the π–π^* transition. Since the relevant internal coordinates R_2, R_3, and R_4 are related to the C–H stretching (see Table 3) and are almost independent of the remaining internal coordinates, the calculated force constants, and therefore the frequencies for these modes are not scaled in the present work.

Below 2000 cm^{-1} there are remaining eight a_1 and eight b_2 modes. The calculated force constants for the internal coordinates of this group, except for the C–H stretching as stated above, are scaled so as to reproduce the experimental Raman frequencies.

In the ca. 1200—1600 cm^{-1} region the totally symmetric modes of Wilson's 7a, 8a, and 19a are likely observed. However, the assignment is not straightforward because these modes depend sensitively on the force constants for the internal coordinates R_1 and R_6; if these constants are reduced (with the scaling factors being 1.27 and 0.81, respectively), the order of the frequency becomes as follows. 8a; 1531 (1519, 1498) cm^{-1}>19a; 1487 (1356, 1263) cm^{-1}>7a; 1379 (1375,

Table 4. Normal Modes of the Phenoxyl-h_5, -d_3, and d_5 Radicals in the Ground State

Mode	Phenoxyl-h_5 Frequency/cm^{-1} Calcd	Phenoxyl-h_5 Frequency/cm^{-1} Exptl	Phenoxyl-h_5 PED/%	Phenoxyl-d_3 Frequency/cm^{-1} Calcd	Phenoxyl-d_3 Frequency/cm^{-1} Exptl	Phenoxyl-d_3 PED/%	Phenoxyl-d_5 Frequency/cm^{-1} Calcd	Phenoxyl-d_5 Frequency/cm^{-1} Exptl	Phenoxyl-d_5 PED/%	Character	Wilson's notation
$1a_1$	3425	—	R_2:60, R_3:28	3404	—	R_3:99	2534	—	R_2:38, R_3:40, R_4:16	C–H stretch	2
$2a_1$	3412	—	R_4:40, R_2:34, R_3:24	2522	—	R_2:97	2517	—	R_4:40, R_2:50	C–H stretch	20a
$3a_1$	3387	—	R_4:50, R_3:46	2509	—	R_4:96	2491	—	R_4:41, R_3:48	C–H stretch	13
$4a_1$	1531	1505	R_6:40, β_3:20, R_1:17	1519	1487	R_6:34, β_3:23, R_1:23	1498	1489	R_6:38, R_1:37	C–C stretch	8a
$5a_1$	1487	—	β_2:60	1356	—	β_2:26, R_5:24, R_6:20	1263	—	β_2:20, β_3:24, R_7:30	C–H bend	19a
$6a_1$	1379	1398	R_1:58, β_3:24	1375	—	R_1:56, β_3:22,	1361	1369	R_1:39, R_5:18, R_6:18	C–O stretch	7a
$7a_1$	1145	1157	β_3:22, R_6:28	1053	1057	β_3:28, R_7:36	840	846	β_3:38, R_7:32, R_5:18	C–H bend	9a
$8a_1$	995	990	R_7:66	878	868	R_7:35, R_6:22, β_2:34	875	865	R_7:15, R_6:26, β_2:42,	C–C stretch	18a
$9a_1$	857	840	R_5:50, α_2:32	800	812	R_5:35, α_2:44	790	796	R_5:20, α_2:53,	Trigonal	1/12
$10a_1$	763	—	R_5:27, α_2:58	753	755	R_5:40, α_2:46	725	732	R_5:38, α_2:37,	Trigonal	12/1
$11a_1$	528	528	α_1:78	516	517	α_1:77,	515	514	α_1:78	CCC bend	6a
$1b_1$	3424	—	R_2:74, R_3:24	3406	—	R_3:99	2529	—	R_2:67, R_3:30	C–H stretch	20b
$2b_1$	3400	—	R_3:73, R_2:25	2523	—	R_2:97	2509	—	R_3:66, R_2:30	C–H stretch	7b
$3b_2$	1565	—	R_5:29, R_7:24, α_3:12	1532	—	R_5:39, R_7:27, α_3:14	1515	—	R_5:42, R_7:27, α_3:13	C–C stretch	8b
$4b_2$	1411	—	R_6:18, β_3:24	1353	—	R_6:26, β_3:52	1285	—	R_6:32, β_1:12, β_4:10	C–H bend	19b
$5b_2$	1349	1331	β_2:44, β_3:26, β_4:18,	1188	—	R_7:25, R_6:42, β_2:16	1054	—	β_2:48, β_3:33, β_4:13	C–H bend	3
$6b_2$	1236	—	R_7:30, R_5:24, R_6:18	1233	—	R_7:32, R_5:34, β_3:16	1212	1234	R_7:40, R_5:16, R_6:33	C–C stretch	14
$7b_2$	1120	—	β_4:24, β_3:21, R_6:22	819	—	β_4:66	814	—	β_4:67	C–H bend	15
$8b_2$	1060	—	R_6:40, β_4:22	937	—	R_6:15, β_4:18, β_2:56	831	—	R_6:16, β_2:34, β_3:40,	C–H bend	18b
$9b_2$	666	—	α_3:77	649	—	α_3:71,	636	—	α_3:71	CCC bend	6b
$10b_2$	426	—	β_1:80	411	—	β_1:77	408	—	β_1:77	C–O bend	9b

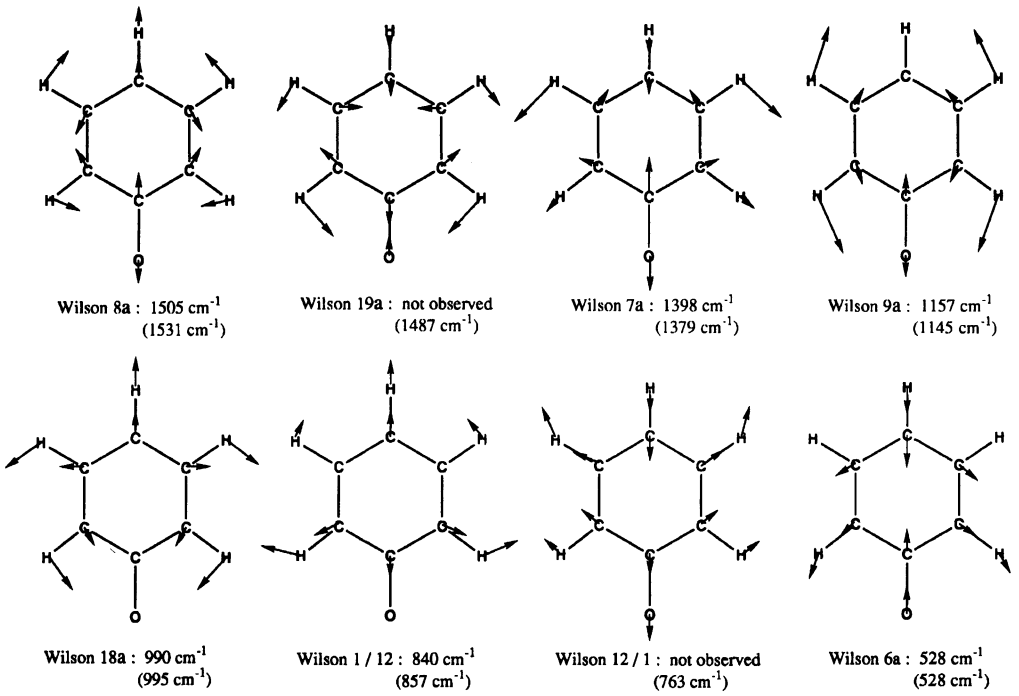

Fig. 3. The normal vibrations of the phenoxyl-h_5 radical in the ground state. The totally symmetric modes, $4a_1$—$11a_1$, are shown with their observed frequencies which are taken from Ref. 38. The values in parentheses are calculated frequencies.

1361) cm^{-1}, those in parentheses being for phenoxyl-d_3 and phenoxyl-d_5. However, if the constants are increased (with the scaling factors of 1.51 and 1.10), the order of 19a and 7a is reversed and we obtain, 8a; 1700 (1691, 1683) cm^{-1}>7a; 1516 (1502, 1488) cm^{-1}>19a; 1419 (1372, 1247) cm^{-1}. In the following the two cases of scaling are called case 1) and case 2) and are discussed comparatively to conclude that case 1) is more plausible.

Case 1): The totally symmetric modes which are strongly enhanced by the resonance are those effective in the nuclear displacement toward the equilibrium molecular geometry in the resonant states. The Raman spectrum observed by the excitation with 399 nm photons[38] are considered to involve the two nearly overlapping excited states, $\tilde{1}^2A_2$ and $\tilde{2}^2B_1$. According to Table 1 the largest change of the internuclear distance upon the excitation of $\tilde{X}\rightarrow\tilde{1}^2A_2$ occurs at R_6(= C_2–C_3) with $\Delta R_6=+0.06$ Å and the second largest at R_1(=C–O) with $\Delta R_1=-0.04$ Å, while upon the excitation of $\tilde{X}\rightarrow\tilde{2}^2B_1$ the largest change occurs at R_1 with $\Delta R_1=+0.07$ Å. As shown in Fig. 3, Wilson's 8a is characterized dominantly by the C_2–C_3 and C–O stretchings. Therefore, it is reasonable to associate this mode with the resonant excitation. In contrast, since Wilson's 7a mode is dominated only by the C–O stretching, it is unlikely that this mode is involved in the resonance enhancement. The remaining Wilson's 19a will not be enhanced significantly because it is dominated by the C–H bending. The scaling of case 1) is also consistent with the effect of deuteration; since Wilson's 8a is mainly characterized by the skeletal change of C_2–C_3 and C–O stretchings, the deuteration effect should be small, which is consistent with the relatively small change of 1505, 1487, and 1489 cm^{-1} in the experimental spectra (see Table 4).

Case 2): In this case the 1700 cm^{-1} band ought to be assigned to Wilson's 8a. However, there is no significantly strong band in this region in the experimental Raman spectrum.[38] This demands that the observed band at 1505 (1487, 1489) cm^{-1} be associated with Wilson's 7a of the C–O stretching character, which is unlikely for the reason mentioned in case 1).

Our favoring of case 1) over case 2) with the order of the frequency of Wilson's 8a>19a>7a for the phenoxyl radical coincides with the order for phenol where the frequencies of 8a, 19a, and 7a are 1609, 1510, and 1255 cm^{-1}, respectively.[50] The values of 1255 cm^{-1} and 1398 cm^{-1} assigned to Wilson's 7a of phenol and the phenoxyl radical, respectively, are reasonable because the C–O bond of phenol is of a single bond character whereas that of the phenoxyl radical is a semi-double. The difference between 1609 cm^{-1} of Wilson's 8a of phenol against 1505 cm^{-1} of the phenoxyl radical may be attributable to the difference in the electronic structure as a whole between the two species.

In the experimental spectrum[38] another weak band is seen at 1331 cm^{-1} for h_5 and 1234 cm^{-1} for d_5 isotopomers in the ca. 1200—1600 cm^{-1} region. Since no totally symmetric mode is left any more in this region according to Table 4, the weak band must be associated with a non-totally symmetric mode. The candidates in

Table 4 are Wilson's 8b, 19b, 3, and 14. A tentative assignment is shown in Table 4 for the two isotopomers.

In the region below ca. 1200 cm^{-1} there are five totally symmetric modes as shown in Table 4. The two modes of the highest and lowest frequencies of 1157 (1057, 865) cm^{-1} and 528 (517, 514) cm^{-1} bands in the experimental spectrum are assigned unambiguously to Wilson's 9a and 6a modes. However, the assignment for the remaining three modes cannot be uniquely carried out because only two are observed at 990 and 840 cm^{-1} for the phenoxyl-h_5 radical. Thus, two scalings are possible depending on the assumption that the undetected band lies below ca. 840 cm^{-1} or above ca. 990 cm^{-1}. The two cases are called case 1) and case 2). In the following we will demonstrate that case 1) is favorable over case 2).

Case 1): In this case the undetected band for phenoxyl-h_5 is predicted to be at 763 cm^{-1} whose character is determined mainly by large PED for α_2 and R_5. The calculated 857 cm^{-1} band which is corresponded to the observed weak 840 cm^{-1} band is also characterized by α_2 and R_5 while the calculated 995 cm^{-1} band to be compared with the observed 990 cm^{-1} band is predominantly characterized by R_7. The fact that only this 990 cm^{-1} band is fairly strong among the three is compatible with the result that the change in $R_7(=C_3-C_4)$ is large for $\tilde{X}\rightarrow\tilde{2}^2B_1$ but not in $R_5(=C_1-C_2)$ for both excitations to $\tilde{1}$ and $\tilde{2}$ as shown in Table 1 (see the discussion of case 2) below also). The observed 812 cm^{-1} and 796 cm^{-1} bands for phenoxyl-d_3 and phenoxyl-d_5 are favorably compared with the calculated 800 cm^{-1} and 790 cm^{-1} bands (see Table 4).

Case 2): In this case the undetected band for phenoxyl-h_5 is predicted at 1024 cm^{-1} with the character of R_7 and α_2. Therefore, if case 2) were true, one should expect the observation of the calculated 1024 cm^{-1} band because it is to be characterized by R_7 and α_2 in common to the observed 990 cm^{-1} band, whereas the observed 840 cm^{-1} band is almost exclusively to be characterized by $R_5(=C_1-C_2)$ alone. However, with the assumption of case 2) the observed weak bands at 812 cm^{-1} and 796 cm^{-1} for phenoxyl-d_3 and phenoxyl-d_5, respectively, cannot be reproduced by the calculation.

Based on the above argument we conclude that case 1) is more realistic. Although the calculated 763 cm^{-1} band for phenoxyl-h_5 is not found in the experimental spectrum probably because of the weakness of intensity, the corresponding calculated bands at 753 cm^{-1} and 725 cm^{-1} for phenoxyl-d_3 and phenoxyl-d_5 are favorably compared with the observed 755 cm^{-1} and 732 cm^{-1} bands (see Table 4). The character of this mode is assigned to a trigonal mode, i.e., a mixture of Wilson's 1 and 12. A similar assignment is made to the observed 840 (812, 796) cm^{-1} bands.

The character of the observed 528 (517, 514) cm^{-1} band assigned to Wilson's 6a is dominated by the internal coordinate α_1 involving the CCC angle of the phenyl ring. In this mode a large nuclear displacement takes place upon both $\tilde{X}\rightarrow\tilde{1}^2A_2$ and $\tilde{X}\rightarrow\tilde{1}^2B_1$ excitations to be easily detected in the resonance Raman experiment.

Tripathi and Schuler recently assigned the observed 1505 and 1398 cm^{-1} bands of phenoxyl-h_5 to Wilson's 7a and 19a, respectively, and the 1552 cm^{-1} band which was reported by Johnson et al.[37] to Wilson's 8a.[39] However, in the present calculation no band which corresponds to the 1552 cm^{-1} band appears and the 1505 and 1398 cm^{-1} bands are reasonably assigned to Wilson's 8a (C–C stretching) and 7a(C–O stretching), respectively, as is described above. The present result is also consistent with the result of the UNO-CAS calculation by Liu and Zhou; a band about 1500 cm^{-1} was due to C–C stretching while the C–O stretching mode was calculated to be about 1400 cm^{-1}.[43]

Normal Modes of the Excited States. The vibrational analysis of the first two excited states, $\tilde{1}^2A_2$, and $\tilde{2}^2B_1$, will be made in this subsection. The phenoxyl radical is the simplest carbonyl containing aromatic radical whose π–π^* excited states are studied by the matrix-isolated electronic absorption spectroscopy by Pullin and Andrews[35] and by Trapped Ion Photodissociation (TIP) spectroscopy by Mikami et al.[40,41] The TIP spectrum is essentially the same as the electronic absorption spectrum so that the vibronic analysis should provide information of the vibrational state of the electronically excited states of the radical in the gas phase. The TIP spectra observed in Refs. 40 and 41 are reproduced in Figs. 4 and 5, respectively. The former spectrum covers the spectral region which, according to the present study, should be regarded as corresponding to $\tilde{X}\rightarrow\tilde{1}^2A_2$ and $\tilde{X}\rightarrow\tilde{2}^2B_1$. The latter spectrum, which covers only the lower energy part of the spectrum in Fig. 4, is recently improved in the spectral resolution.[41] Although even the improved resolution in Ref. 41 is still much lower than the simplest carbonyl containing aliphatic radical, i.e., the vinyloxyl radical which has been studied extensively,[49] we attempt to analyze the vibrational structure of the phenoxyl radical as much as possible.

In order to scale properly the force constants in the electronic excited states the TIP vibronic spectrum must be correctly assigned. The force fields of the $\tilde{X}^2B_1$, $\tilde{1}^2A_2$, and $\tilde{2}^2B_1$ states are expected to be appreciably different with each other because the geometries of the state are considerably different as shown in Table 1. Therefore, the Dushinsky effect is considered to be significant. Moreover, in reference to the case of the benzyl radical it is conceivable that an extensive vibronic coupling makes the vibronic assignment formidable. Despite this easily foreseeable difficulty we first calculate the Franck–Condon integrals for the two transitions independently by including the Duschinsky effect.

The relative intensities of the vibronic bands are calculated by Eq. 12.

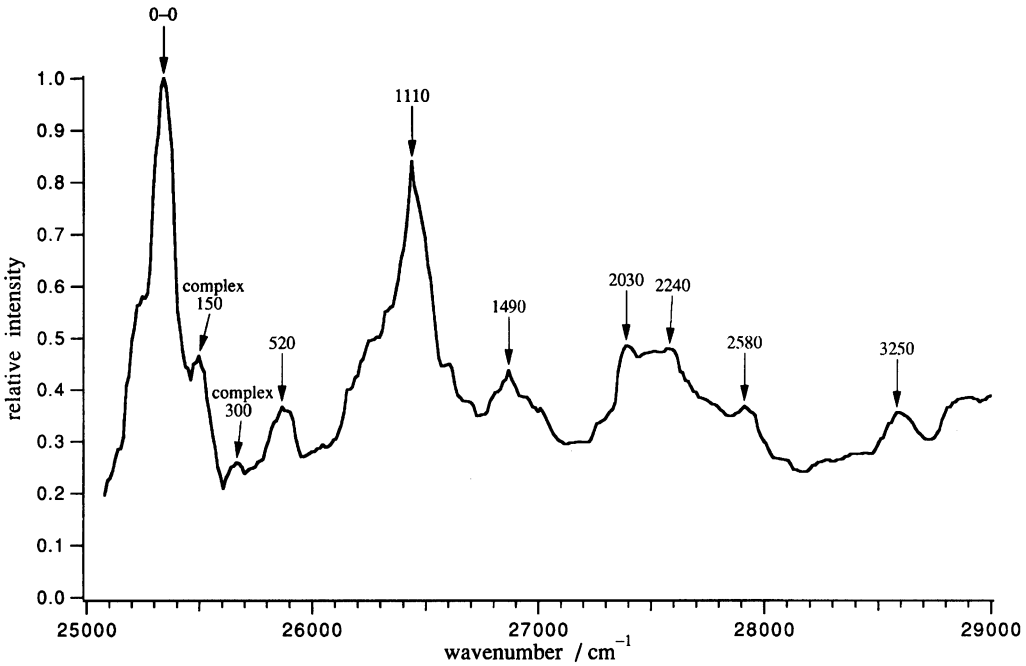

Fig. 4. TIP spectrum of $[C_6H_5OH–N(CH_3)_3]^+(1)$. This spectrum is taken from Ref. 40 and replotted in units of wavenumber.

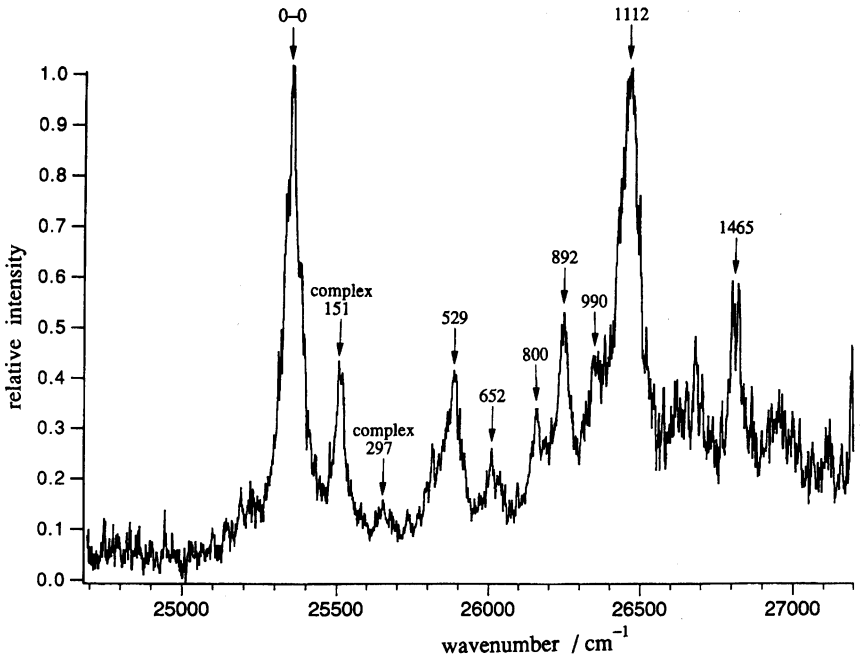

Fig. 5. TIP spectrum of $[C_6H_5OH–N(CH_3)_3]^+(2)$. This spectrum is taken from Ref. 41, where the spectral resolution is improved in the region lower than ca. 27000 cm^{-1}.

$$I_m = (E_0 + \varepsilon_m) \mid J(\{{}^{m}_{0}\}) \mid^2 \tag{12}$$

where $J(\{{}^{m}_{0}\})$ is the Franck–Condon integral for the excitation from the zero-point vibrational state of the ground electronic state to a vibrational state $\{m\}$ of the excited electronic state. The symbols E_0 and ε_m are the 0–0 electronic excitation energy and the vibrational energy level for the $\{m\}$ state, respectively.

In Figs. 4 and 5 the strongest band is at 25, 350 cm^{-1} (ca. 395 nm). In Fig. 4 other maxima occur at ca. 520 cm^{-1}, ca. 1110 cm^{-1}, ca. 1490 cm^{-1} ca. 2030 cm^{-1}, ca. 2240 cm^{-1}, ca. 2580 cm^{-1}, and ca. 3250 cm^{-1} relative to the strongest band. In Fig. 5 better resolved maxima are seen at 529 cm^{-1}, 652 cm^{-1}, 800 cm^{-1}, 892 cm^{-1}, 990 cm^{-1}, 1112 cm^{-1}, and 1465 cm^{-1}. Among them the maxima at ca. 1110 cm^{-1} (1112 cm^{-1}) is the second strongest. The small peaks at ca. 150 cm^{-1} (151 cm^{-1})

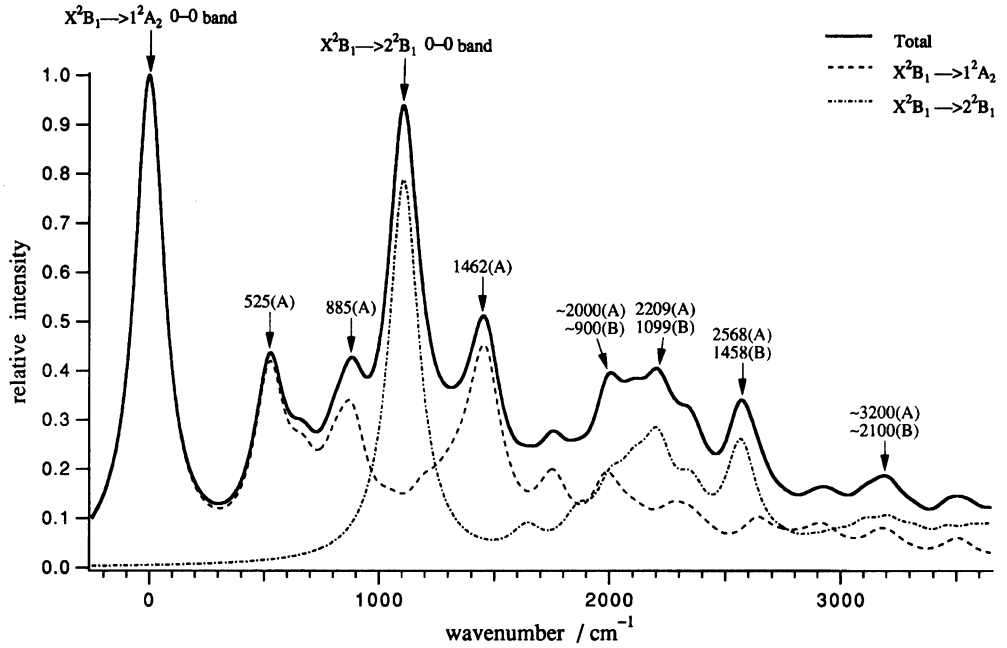

Fig. 6. Calculated vibronic absorption spectrum(1) to be compared with the spectrum in Fig. 4. The spectra for $\tilde{X}^2B_1 \rightarrow \tilde{1}^2A_2$ (broken curve) and $\tilde{X}^2B_1 \rightarrow \tilde{2}^2B_1$ (dash-and-dot curve) calculated independently and broadened with a Lorentzian linewidth of 80 cm^{-1} are overlapped with the ratio of the two 0–0 bands as 100 : 80 to yield the solid curve. The absorption intensities are calculated by Eq. 12 using the Franck–Condon integrals after the scaling of the geometry. The values with A and B in parentheses denote the wavenumbers which are measured from the 0–0 bands of $\tilde{X}^2B_1 \rightarrow \tilde{1}^2A_2$ and $\tilde{X}^2B_1 \rightarrow \tilde{2}^2B_1$, respectively.

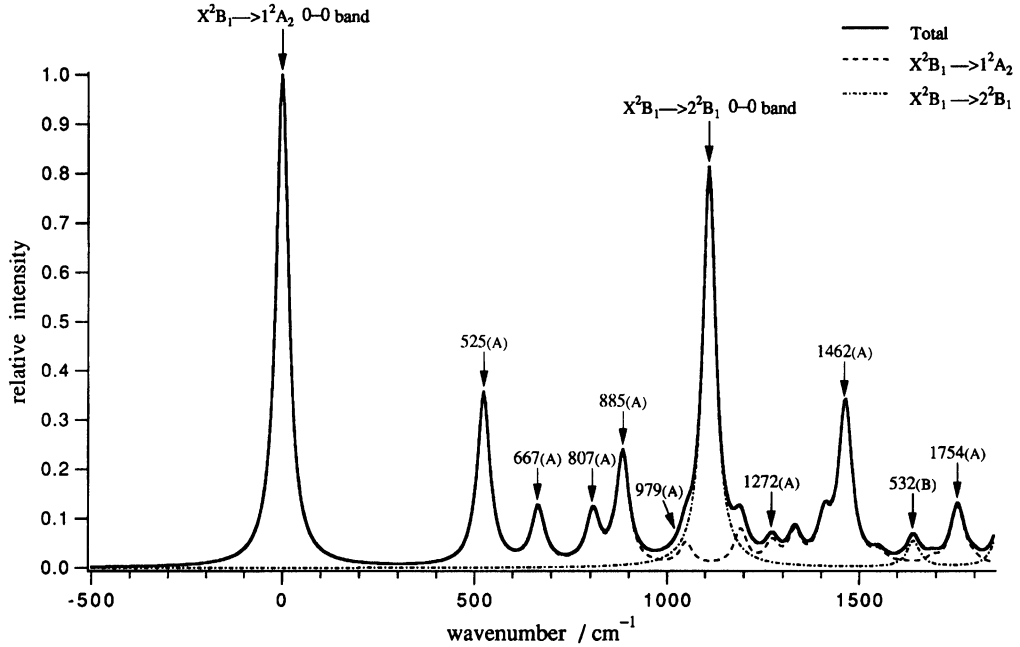

Fig. 7. Calculated vibronic absorption spectrum(2) to be compared with the spectrum in Fig. 5. Same as Fig. 6 except that the Lorentzian linewidth is taken to be 20 cm^{-1}.

and ca. 300 cm^{-1} (297 cm^{-1}) have been attributed to the intermolecular vibrational modes of the complex between the phenoxyl radical and the counterpart protonated amines inherent in the TIP experiment[41] so that they are neglected in the present study of the free phenoxyl radical.

The attempt to reproduce the observed TIP spectrum by assuming forcedly that the spectrum consisted of only a single transition of $\tilde{X} \rightarrow \tilde{1}^2A_2$ or $\tilde{X} \rightarrow \tilde{2}^2B_1$ failed despite our repeated trials of scaling the force constants

Table 5. Normal Modes of the Phenoxyl-h_5 Radical in the Excited States

Mode	Wilson's notation	$\tilde{1}^2A_2$ state Frequency/cm^{-1} Calcd	Exptl	PED/%	$\tilde{2}^2B_1$ state Frequency/cm^{-1} Calcd	Exptl	PED/%
$1a_1$	2	3434	—	R_4:29, R_2:36, R_3:32	3758	—	R_4:74
$2a_1$	20a	3422	—	R_4:35, R_2:57	3742	—	R_2:56, R_3:20, R_4:22
$3a_1$	13	3396	—	R_4:33, R_3:60	3728	—	R_3:60, R_2:35
$4a_1$	8a	1754	—	R_1:53, R_5:26	1901	—	R_1:23, R_5:33
$5a_1$	19a	1462	1465	R_1:16, R_7:34, R_6:30	1458	1470 (2580)	β_3:33, R_7:32
$6a_1$	7a	1272	—	R_1:18, R_7:22, R_5:24	1244	—	β_2:36, R_1:30, R_6:24
$7a_1$	9a	979	990	β_3:60, R_7:32	1099	1130 (2240)	β_3:52, β_2:22
$8a_1$	18a	885	892	R_5:36, R_6:28	998	—	R_7:40, R_6:28, β_2:26
$9a_1$	1/12	807	800	β_2:80	896	920 (2030)	α_2:27, R_5:30
$10a_1$	12/1	667	652	α_1:31, α_2:51	753	—	α_1:23, α_2:58
$11a_1$	6a	525	529	α_1:39, α_2:39	532	—	α_1:60

The values in parentheses are in wavenumbers which are measured from the 0–0 band of $\tilde{X}^2B_1 \rightarrow \tilde{1}^2A_2$.

of each state; in the assumption that the spectrum was solely due to a single transition of $\tilde{X} \rightarrow \tilde{1}^2A_2$ fairly strong bands at ca. 500 cm^{-1} and ca. 1500 cm^{-1} could be predicted but not the one at ca. 1000 cm^{-1}. Similarly, in another assumption that only $\tilde{X} \rightarrow \tilde{2}^2B_1$ was responsible fairly strong bands could be expected at ca. 1000 cm^{-1} and ca. 1500 cm^{-1} but not at ca. 500 cm^{-1}, in contradiction to the experimental spectrum. However, the simple superposition of the two curves with the strongest band assigned to the 0–0 band of $\tilde{X} \rightarrow \tilde{1}^2A_2$ and the second strongest at ca. 1110 cm^{-1} in Fig. 4 and 1112 cm^{-1} in Fig. 5 to the 0–0 band $\tilde{X} \rightarrow \tilde{2}^2B_1$ reproduces fairly well the experimental TIP spectrum (as shown in the solid curve in Fig. 6). Furthermore, the spacing of ca. 1110 cm^{-1} between the two assumed 0–0 bands is roughly compatible with the calculated difference of the energy between the two transitions, which is 1234 cm^{-1} according to the result of method (3) in Table 2.

As far as we rely on our interpretation that the TIP spectrum is just an overlap of the two transitions, the observed bands in Fig. 5 are assignable to the fundamental vibronic bands of $\tilde{X} \rightarrow \tilde{1}^2A_2$ expect that the one at 1112 cm^{-1} is due to the transition of $\tilde{X} \rightarrow \tilde{2}^2B_1$. In the region from ca. 1600 cm^{-1} to ca. 3000 cm^{-1} in Fig. 4 overtone or combination bands of $\tilde{X} \rightarrow \tilde{1}^2A_2$ and a few fundamental bands of $\tilde{X} \rightarrow \tilde{2}^2B_1$ are probably seen as indicated by the broken and dash-and-dot curves of Fig. 6.

Except for the modes higher than 3000 cm^{-1} (see Normal Modes of the Ground State) the scaling for the force constants of the two excited states yields the result in Table 5 which shows that the notations of the normal modes are in parallel with those of the ground state given in Table 4 except that the feature of the PED differs probably due to the difference in the geometry of the excited states and the ground state.

The intensities of the vibronic bands relative to the 0–0 band as calculated by Eq. 11 are found to be larger than those in the experimental spectrum. For example, the calculated relative intensities for the observed 529

Table 6. Calculated Vibronic Absorption Spectrum

Wavenumber cm^{-1}	Relative intensity	Mode
0	1.000	$\tilde{1}^2A_2$ 0–0 band
525	0.352	$\tilde{1}^2A_2$ $11a_1$
667	0.115	$\tilde{1}^2A_2$ $10a_1$
807	0.102	$\tilde{1}^2A_2$ $9a_1$
885	0.223	$\tilde{1}^2A_2$ $8a_1$
979	0.001	$\tilde{1}^2A_2$ $7a_1$
1050	0.045	$\tilde{1}^2A_2$ $11a_1 \times 2$
1110	0.800	$\tilde{2}^2B_1$ 0–0 band
1192	0.071	$\tilde{1}^2A_2$ $10a_1+11a_1$
1272	0.043	$\tilde{1}^2A_2$ $6a_1$
1332	0.060	$\tilde{1}^2A_2$ $9a_1+11a_1$
1410	0.082	$\tilde{1}^2A_2$ $8a_1+11a_1$
1463	0.304	$\tilde{1}^2A_2$ $5a_1$
1642	0.052	$\tilde{2}^2B_1$ $11a_1$
1754	0.108	$\tilde{1}^2A_2$ $4a_1$
1863	0.067	$\tilde{2}^2B_1$ $10a_1$
1987	0.110	$\tilde{1}^2A_2$ $5a_1+11a_1$
2006	0.107	$\tilde{2}^2B_1$ $9a_1$
2108	0.105	$\tilde{2}^2B_1$ $8a_1$
2209	0.189	$\tilde{2}^2B_1$ $7a_1$
2347	0.055	$\tilde{1}^2A_2$ $5a_1+8a_1$
2354	0.103	$\tilde{2}^2B_1$ $6a_1$
2568	0.220	$\tilde{2}^2B_1$ $5a_1$
2639	0.043	$\tilde{1}^2A_2$ $4a_1+8a_1$
2924	0.043	$\tilde{1}^2A_2$ $5a_1 \times 2$
3011	0.001	$\tilde{2}^2B_1$ $4a_1$
3105	0.030	$\tilde{2}^2B_1$ $7a_1+9a_1$
3207	0.050	$\tilde{2}^2B_1$ $7a_1+8a_1$
3216	0.030	$\tilde{1}^2A_2$ $4a_1+5a_1$
3508	0.034	$\tilde{1}^2A_2$ $4a_1 \times 2$
3566	0.036	$\tilde{2}^2B_1$ $5a_1+8a_1$
3667	0.052	$\tilde{2}^2B_1$ $5a_1+7a_1$

The stick spectrum for Fig. 6 is shown, where the peaks for the fundamental bands and the peaks whose intensities are more than 0.03 are listed.

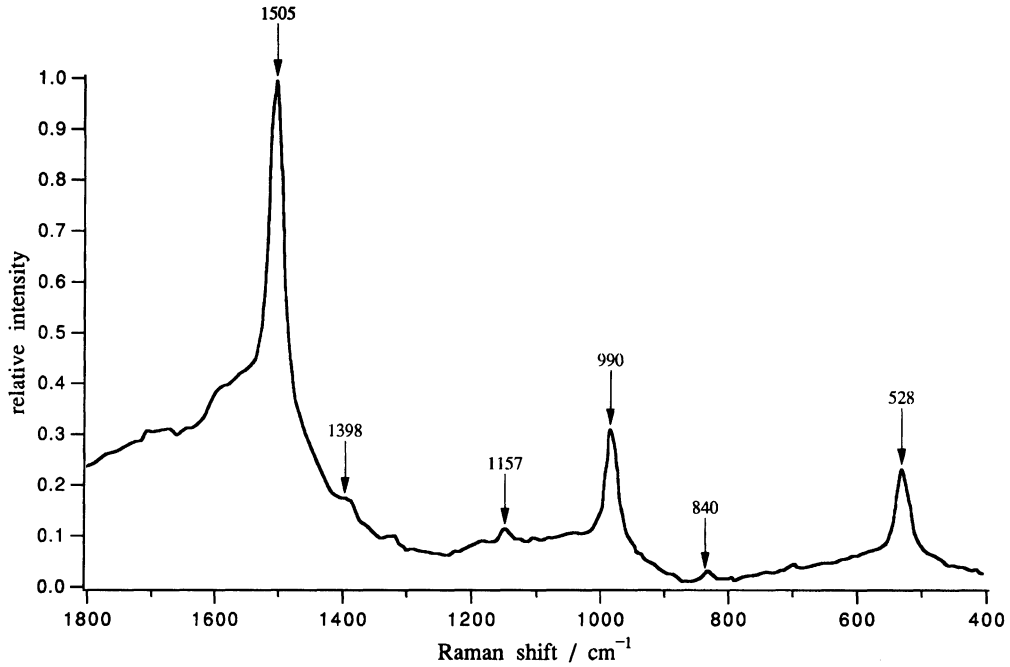

Fig. 8. Experimental Raman spectrum. Transient Raman spectrum of the phenoxyl-h_5 radical resonanced at 399 nm which is taken from Ref. 38.

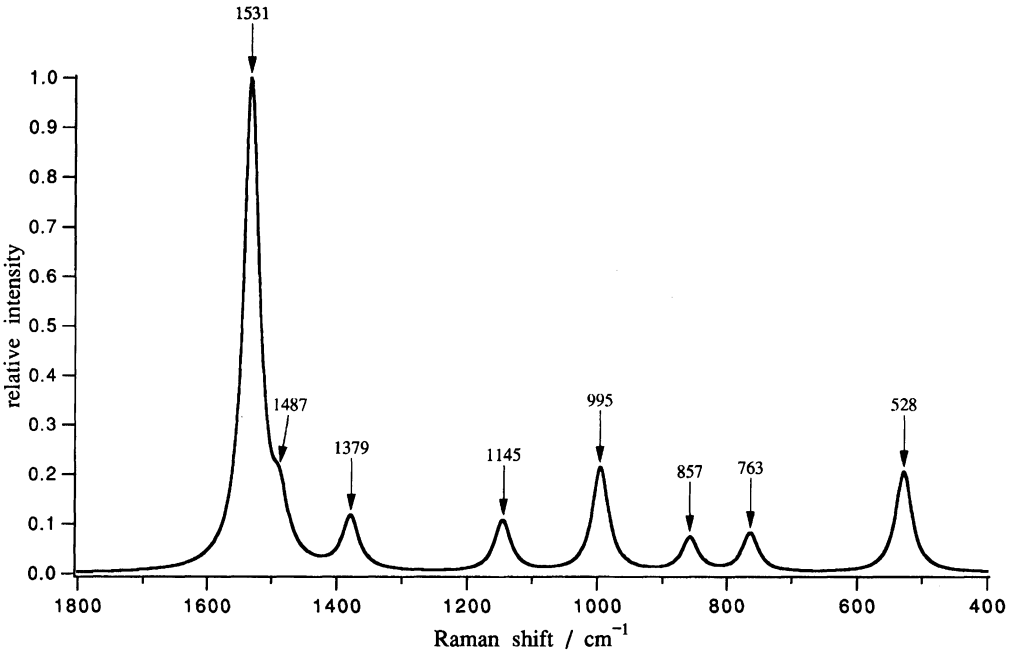

Fig. 9. Calculated Raman spectrum. The Raman intensities calculated by Eq. 15 using the Franck–Condon integrals obtained under the same condition as in the calculation of the absorption spectrum.

cm^{-1} and 1465 cm^{-1} bands of the $\tilde{1}^2A_2$ state against the 0–0 band are ca. 60 : 100 and ca. 70 : 100 as compared with ca. 35 : 100 and ca. 45 : 100 in the TIP spectrum. This overestimation will be argued in the following.

The intensities of the 0→1 and 0–0 bands are related by Eq. 13 derived from Eq. 10.

$$\boldsymbol{J}(^{m_\mu=1}_{0}) = \frac{1}{\sqrt{2}} d_\mu \boldsymbol{J}(^{0}_{0}) \tag{13}$$

Thus, the relative intensity for $0 \rightarrow m_\mu = 1$ is proportional to the coefficient d_μ. If $\boldsymbol{W} \sim \boldsymbol{1}$, then

$$d_\mu \cong \tilde{\kappa}_\mu = \gamma_\mu^{\frac{1}{2}} k_\mu \tag{14}$$

Therefore, the relative intensity for $0 \rightarrow m_\mu = 1$ is proportional to the k-vector which is a measure of the molecular geometry change following the electronic excitation. We have modified the vectors, which may be

Table 7. Calculated Raman Spectrum

Mode	Raman shift/cm^{-1} Calcd	Exptl	Relative intensity	Division of the relative intensity $\tilde{X}^2B_1 \rightarrow \tilde{1}^2A_2$	$\tilde{X}^2B_1 \rightarrow \tilde{2}^2B_1$
$4a_1$	1531	1505	1.0000	0.9087	0.0913
$5a_1$	1487	—	0.1080	0.1006	0.0074
$6a_1$	1379	1398	0.1072	0.0519	0.0553
$7a_1$	1145	1157	0.1047	0.1043	0.0004
$8a_1$	995	990	0.2136	0.1750	0.0386
$9a_1$	857	840	0.0689	0.0242	0.0447
$10a_1$	763	—	0.0788	0.0220	0.0568
$11a_1$	528	528	0.2064	0.1809	0.0255

called "scaling of the geometry factor", to give the best fit to the experimental relative vibronic intensities. As a result, the factor is chosen to be 0.8. With this adjustment the calculated relative intensities for the observed 529 cm^{-1} and 1465 cm^{-1} bands against the 0–0 band turn out to be ca. 40 : 100 and ca. 50 : 100.

The calculated vibronic absorption spectra are shown in Figs. 6 and 7 where each peak is broadened with a Lorentzian linewidth of 80 cm^{-1} and 20 cm^{-1}, respectively. In both spectra the ratio of the 0–0 bands is taken to be 100 : 80 rather arbitarily, which is not so badly far from the ratio of the calculated oscillator strengths in Table 2. Table 6 lists a part of the stick spectrum for Fig. 6.

The fair agreement of the spectra between the experiment and calculation is remarkable in view of the fact that the theoretical spectrum is obtained only by a simple superposition of the two vibronic spectra for $\tilde{X} \rightarrow \tilde{1}^2A_2$ and $\tilde{X} \rightarrow \tilde{2}^2B_1$ without taking into account the vibronic coupling between the two excitations. We attempt to rationalize this result as follows: In the benzyl radical a strong vibronic coupling between $\tilde{1}^2A_2$ and $\tilde{2}^2B_1$ gives an extremely complicated spectral feature.[8,13] However, there is a relieving fact reported by Fukushima and Obi,[15] that is, if the energy separation between the two states of the benzyl is increased from ca. 450 cm^{-1} to ca. 1000 cm^{-1} by a moderate perturbation such as the fluorination at the para position of the benzyl radical, the spectral feature of the *p*-fluorobenzyl radical becomes dramatically simple, which is attributed to the vanishment of the vibronic coupling prominent in the prototype benzyl radical. As for the phenoxyl radical the energy difference between the two transitions is calculated as 1234 cm^{-1} by method (3) (see Table 2) which is roughly compatible with the experimental values of ca. 1110 cm^{-1} in Fig. 4 or 1112 cm^{-1} in Fig. 5. Thus, by analogy with the benzyl systems we may conceive that the two excited states of the phenoxyl radical are separated enough to vanish the vibronic coupling. It is desired to perform spectroscopic experiments to determine the polarization of the two transitions.

Raman Spectrum. The Raman spectrum induced by the resonance to the ca. 400 nm band is calculated by using the same set of the force constants and the Franck–Condon integrals as in the absorption spectrum. The relative intensities, I, of the Raman spectrum are calculated in terms of the Albrecht A-term[51] by Eq. 15.

$$I = E_L E_S^3 \left\{ \left| M_A^2 \sum_{m^A}^{A} \frac{J(m_f^A) J(m_0^A)}{\varepsilon_m^A + E_0^A - E_L - i\Gamma} \right|^2 + \left| M_B^2 \sum_{m^B}^{B} \frac{J(m_f^B) J(m_0^B)}{\varepsilon_m^B + E_0^B - E_L - i\Gamma} \right|^2 \right\} \quad (15)$$

E_L and E_S are the incident and scattered photon energies. M_A and M_B are the transition moments for the excitations, $\tilde{X} \rightarrow \tilde{1}^2A_2$ and $\tilde{X} \rightarrow \tilde{2}^2B_1$, respectively. The symbols m^A and m^B represent the intermediate vibrational states belonging to the $\tilde{1}^2A_2$ and $\tilde{2}^2B_1$ states, respectively, which include the fundamental, overtone, and combination states, and ε_m^A and ε_m^B represent the vibrational energy. In the present calculation the number of the intermediate states amounts to be 281 between the initial (0) and the final (f) states. E_0^A and E_0^B are the 0–0 excitation energies for $\tilde{X} \rightarrow \tilde{1}^2A_2$ and $\tilde{X} \rightarrow \tilde{2}^2B_1$. Γ is the homogeneous linewidth.

The experimental Raman spectrum of the phenoxyl radical excited at 399 nm by Tripathi and Schuler[38] is shown in Fig. 8, the calculated one in Fig. 9 and Table 7. The values of M_A and M_B are set as $M_A : M_B = 10 : 9$ to be consistent with the oscillator strengths in the calculated vibronic absorption spectrum where the ratio of the 0–0 bands is chosen to be 100 : 80. The value of E_L is fixed to 25000 cm^{-1} (=ca. 399 nm). The value of E_0^B is taken to be larger by 1110 cm^{-1} than E_0^A, and E_0^A is regarded as a parameter along with Γ so as to reproduce the experimental Raman spectrum. For the best fit of Fig. 9 to Fig. 8 E_0^A and Γ are chosen as 23610 cm^{-1} (=ca. 423 nm) and 70 cm^{-1}, respectively, with each peak being broadened by the Lorentzian inhomogeneous linewidth of 15 cm^{-1}. The value of 423 nm for E_0^A is reasonable because the edge of the absorption of the 400 nm band is located at about 420 nm. Also, an emission is observed in the ca. 420—440 nm region in Raman spectroscopy.[38]

Since there is some background emission in the experimental Raman spectrum, it is not straightforward to compare the experimental and calculated spectra. Nev-

erthelss, the calculated spectrum in Fig. 9 reproduces fairly well the general character of the experimental, i. e., the very strong band at 1505 cm^{-1} followed by those at 990 and 528 cm^{-1}. The intensity of the 1487 cm^{-1} band is calculated to be considerably large but the band seems to be buried under the very strong 1531 cm^{-1} band. As shown in the fifth and sixth columns of Table 7 the strong bands at 1531, 995, and 528 cm^{-1} are mainly dominated by the $\tilde{1}^2A_2$ state, while in the weak bands at 1379, 857, and 763 cm^{-1} the contribution of the $\tilde{2}^2B_1$ state cannot be negligible.

Conclusion

The electronic and vibrational structures of the ground and the first two π–π^* excited states of phenoxyl radical are studied by the ab initio MO method. The electronic excitation energies and transition dipole moments are calculated for the optimized geometry by the CAS-MCSCF and CI procedures with Huzinaga–Dunning DZV basis set. The force constants for the ground and the excited states are calculated and the vibrational analysis of the three states is carried out. The Franck–Condon integrals for the two π–π^* transitions are also calculated to compare the TIP spectrum.[52] Similarly, the theoretical Raman spectrum is compared with the experimental spectrum. The results are summarized as below.

(1) The electronic absorption band at about 600 nm is assigned to the $\tilde{X}^2B_1 \rightarrow \tilde{1}^2B_2$ ($n \rightarrow \pi$) transition while the absorption at ca. 400—300 nm is assigned to the overlapped absorption of $\tilde{X}^2B_1 \rightarrow \tilde{1}^2A_2$ and $\tilde{X}^2B_1 \rightarrow \tilde{2}^2B_1$. The absorption at shorter than ca. 300 nm band is assigned to the $\tilde{X}^2B_1 \rightarrow \tilde{2}^2A_2$.

(2) The normal modes for the ground state of the phenoxyl radical are assigned as follows; the totally symmetric modes are Wilson's 8a (1505 cm^{-1}), 19a (1487 cm^{-1}), 7a (1398 cm^{-1}), 9a (1157 cm^{-1}), 18a (990 cm^{-1}), 1/12 (840 cm^{-1}), 12/1 (763 cm^{-1}), and 6a (528 cm^{-1}). The 8a mode enhanced most strongly is characterized as a phenyl ring stretching while the 7a mode as the C–O stretching.

(3) In the TIP spectrum the strongest band is assigned to the 0–0 band of $\tilde{X} \rightarrow \tilde{1}^2A_2$. The second strongest located at 1110 cm^{-1} higher than the former is assigned to the 0–0 band of $\tilde{X} \rightarrow \tilde{2}^2B_1$. All the remaining peaks are assigned to belong either the former or the latter electronic transition.

(4) The TIP spectrum is reproduced by simply overlapping the vibronic spectra of $\tilde{X} \rightarrow \tilde{1}^2A_2$ and $\tilde{X} \rightarrow \tilde{2}^2B_1$, which is attributed to a large enough energy separation between the two electronic states.

The authors are grateful to Dr. Makoto Yamaguchi for his helpful advice on the calculation of the Franck–Condon integrals. Mr. Shin Sato, Professors Takayuki Ebata and Naohiko Mikami kindly provided us pertinent experimental data of the TIP spectrum of Fig. 5. We are also grateful to Dr. G. N. R. Tripathi and Professor R. H. Schuler for their providing us pertinent information of the Raman spectrum of the phenoxyl radical. Numerical calculations were performed at the Computer Center of the Kyoto University and at the IMS Computer Center. The present study was partially supported by Grants-in-Aid for Scientific Research on Priority Areas Nos. 0424203, 05233108, and 05237106 from the Ministry of Education, Science and Culture.

References

1) R. Disselkamp and E. R. Bernstein, *J. Chem. Phys.*, **98**, 4339 (1993).
2) G. Porter and I. Norman, *Proc. R. Soc. London, Ser. A*, **230**, 399 (1953).
3) G. Porter and F. J. Wright, *Trans. Faraday Soc.*, **51**, 1469 (1955).
4) G. Porter and M. W. Windsor, *Nature (London)*, **180**, 187 (1957).
5) G. Porter and E. Strachan, *Spectrochim. Acta*, **12**, 299 (1958).
6) C. Cossart-Magos and S. Leach, *J. Chem. Phys.*, **56**, 1534 (1972).
7) D. M. Friedrich and A. C. Albrecht, *J. Chem. Phys.*, **58**, 4766 (1973).
8) C. Cossart-Magos and S. Leach, *J. Chem. Phys.*, **64**, 4006 (1976).
9) T. Ebata, K. Obi, and I. Tanaka, *Chem. Phys. Lett.*, **77**, 480 (1981).
10) M. Heaven, L. Dimauro, and T. A. Miller, *Chem. Phys. Lett.*, **95**, 347 (1983).
11) N. Ikeda, N. Nakashima, and K. Yoshihara, *J. Chem. Phys.*, **82**, 5285 (1985).
12) M. A. Hoffbauer and J. W. Hudgens, *J. Phys. Chem.*, **89**, 5152 (1985).
13) C. Cossart-Magos and W. Goetz, *J. Mol. Spectrosc.*, **115**, 366 (1986).
14) J. I. Selco and P. G. Carrick, *J. Mol. Spectrosc.*, **137**, 13 (1989).
15) M. Fukushima and K. Obi, *J. Chem. Phys.*, **93**, 8488 (1990).
16) H.-S. Im and E. R. Bernstein, *J. Chem. Phys.*, **95**, 6326 (1991).
17) M. Fukushima and K. Obi, *J. Chem. Phys.*, **96**, 4224 (1992).
18) H. C. Longuett-Higgins and J. A. Pople, *Proc. Phys. Soc. London, Ser. A*, **68**, 591 (1955).
19) W. Bingel, *Z. Naturforsch. A*, **10A**, 462 (1955).
20) J. C. Shug and D. H. Phillips, *J. Chem. Phys.*, **49**, 3734 (1968).
21) N. Kanamaru and S. Nagakura, *Bull. Chem. Soc. Jpn.*, **43**, 3443 (1970).
22) H. M. Chang and H. H. Jaffe, *Chem. Phys. Lett.*, **23**, 341 (1974).
23) J. Wasilewski, *Acta Phys. Pol. A*, **A46**, 341 (1974).
24) G. Orlandi, G. Poggi, and F. Zerbetto, *Chem. Phys. Lett.*, **115**, 253 (1985).
25) J. E. Rice, N. C. Handy, and P. J. Knowles, *J. Chem. Soc., Faraday Trans.*, **83**, 1643 (1987).
26) F. Negri, G. Orlandi, F. Zerbetto, and M. Z. Zgierski,

J. Chem. Phys., **93**, 600 (1990).
27) H. Paul and H. Fischer, *Helv. Chim. Acta*, **56**, 1575 (1973).
28) H. Langhals and H. Fischer, *Chem. Ber.*, **111**, 543 (1978).
29) M. Lehni, H. Schuh, and H. Fischer, *Int. J. Chem. Kinet.*, **11**, 705 (1979).
30) C. Huggenberger and H. Fischer, *Helv. Chim. Acta*, **64**, 338 (1981).
31) G. Porter and E. Strachan, *Trans. Faraday Soc.*, **54**, 1595 (1958).
32) E. J. Land, G. Porter, and E. Strachan, *Trans. Faraday Soc.*, **56**, 1885 (1960).
33) J. L. Roebber, *J. Chem. Phys.*, **37**, 1974 (1962).
34) B. Ward, *Spectrochim. Acta. Part A*, **24A**, 813 (1967).
35) D. Pullin and L. Andrews, *J. Mol. Struct.*, **95**, 181 (1982).
36) S. M. Beck and L. E. Brus, *J. Chem. Phys.*, **76**, 4700 (1982).
37) C. R. Johnson, M. Ludwig, and S. A. Asher, *J. Am. Chem. Soc.*, **108**, 905 (1986).
38) G. N. R. Tripathi and R. H. Schuler, *J. Chem. Phys.*, **81**, 113 (1984).
39) G. N. R. Tripathi and R. H. Schuler, *J. Phys. Chem.*, **92**, 5129 (1988).
40) N. Mikami, T. Sasaki, and S. Sato, *Chem. Phys. Lett.*, **180**, 431 (1991).
41) S. Sato, T. Ebata, and N. Mikami, "Symposium on Molecular Structures," Hiroshima, Oct., 1993.
42) V. B. Luzhkov and A. S. Zyubin, *J. Mol. Struct.*, **170**, 33 (1988).
43) R. Liu and X. Zhou, *J. Phys. Chem.*, **97**, 9613, 9618 (1993).
44) M. Dupuis et al., HONDO : Version 7.0 (1987) QCPE 544.
45) E. R. Davidson et al., "Quantum Chemistry Group," Indiana University (1988), QCPE 580.
46) I. H. Williams, *J. Mol. Struct.*, **94**, 275 (1983).
47) P. Pulay, G. Fogarasi, F. Pang, and J. E. Boggs, *J. Am. Chem. Soc.*, **101**, 2550 (1979).
48) T. Momose and T. Shida, to be published.
49) M. Yamaguchi, T. Momose, and T. Shida, *J. Chem. Phys.*, **93**, 4223 (1990).
50) G. N. R. Tripathi, *J. Chem. Phys.*, **71**, 4025 (1979).
51) A. C. Albrecht, *J. Chem. Phys.*, **34**, 1476 (1961).
52) Recently, the geometry and fundamental vibrations of the phenoxyl radical in the ground electronic state are calculated by D. M. Chipman, R. Liu, X. Zhou, and P. Pulay who have employed the UNO-CAS procedure using the 6-311G (2d, p) basis set. The authors are grateful to Dr. Chipman for his sending a preprint of their work.